



Role of Eddy Heat Feedback in Modulating Winter-Mean NAO-Related Thermodynamic Structure

Shuo ZHAO¹, Hong-Li REN^{1,2,3*}, Fang ZHOU^{4,5}, and Li GAO⁶

¹ Chinese Academy of Meteorological Sciences, Beijing 100081, China.

² Laboratory for Climate Studies & CMA-NJU Joint Laboratory for Climate Prediction Studies, National Climate Center, China Meteorological Administration, Beijing 100081, China.

³ Department of Atmospheric Science, School of Environmental Studies, China University of Geoscience, Wuhan 430074, China.

⁴ Climate Change Research Center, Institute of Atmospheric Physics, and Nansen–Zhu International Research Centre, Chinese Academy of Sciences, Beijing 100029, China.

⁵ Collaborative Innovation Center on Forecast and Evaluation of Meteorological Disasters/Key Laboratory of Meteorological Disaster, Ministry of Education, Nanjing University of Information Science and Technology, Nanjing 210044, China.

⁶ CMA Numerical Prediction Center, National Meteorological Center, Beijing 100081, China.

Corresponding author: Hong-Li Ren, 46 Zhongguancun Nandajie St., Haidian District, Beijing 100081, China. (renhl@cma.gov.cn)

This article has been accepted for publication and undergone full peer review but has not been through the copyediting, typesetting, pagination and proofreading process which may lead to differences between this version and the Version of Record. Please cite this article as doi: 10.1029/2019JD031990

Key Points:

- The low-frequency NAO flow can clearly regulate the eddy-heat flux in the whole troposphere.
- The meridional shifting of eddy potential temperature structure is primarily responsible for generating the eddy-heat feedback onto NAO.
- The positive NAO phase has a negatively stronger eddy-heat feedback than the negative phase.

Accepted Article

Abstract

The thermodynamic structure of the North Atlantic Oscillation (NAO), in terms of the pattern of the winter-mean potential temperature (PT) anomaly in the troposphere, is a crucial indicator of regional climate variations, and can be influenced by synoptic-scale eddy heat (EH) fluxes. The role and mechanism of EH feedback in modulating the winter-mean thermodynamic structure of the NAO are investigated. We show that the low-frequency NAO-related flow can barotropically regulate EH flux and give rise to an EH transport that is down-gradient (up-gradient) of the NAO-related PT anomalies, thus creating negative (positive) EH feedback on PT anomalies in the middle-lower (upper) troposphere. Using eddy structure decomposition, we calculated the two primary terms of anomalous EH flux: the BA term is the product of basic eddy velocity and anomalous eddy PT, and the AB term is the product of anomalous eddy velocity and basic eddy PT. The meridional BA EH flux is caused by the meridional shift of eddy PT structure under NAO. It is a major contributor of the anomalous EH flux and forcing, which weaken NAO-related PT anomalies. The zonal AB EH flux is smaller in magnitude, and is induced by the zonal slant of the eddy streamfunction structure in the negative NAO phase. It creates EH feedback upstream of the NAO flow. In addition, the positive NAO phase has a negatively stronger EH feedback than the negative phase; this is related to the higher persistence of the anomalous PT pattern under negative NAO.

1 Introduction

The North Atlantic Oscillation (NAO), considered as the dominant mode of low-frequency (LF) climate variability over the North Atlantic (Barnston & Livezey, 1987; Loon & Rogers, 1978; Wallace & Gutzler, 1981), strongly influences regional and even Northern Hemispheric weather and climate (Hurrell, 1995a; Hurrell & Deser, 2009; Hurrell et al., 2003; Marshall et al., 2001; Ogi et al., 2003; Sung et al., 2006; Zuo et al., 2013, 2016). Many characteristics of the NAO have been identified in in-depth studies. For example, studies have shown that the negative phase of the NAO is larger in amplitude and higher in persistence than the positive phase (Barnes & Hartmann, 2010; Luo et al., 2018; Woollings et al., 2010); the two phases have different background states (e.g., North Atlantic jet and meridional potential vorticity gradient) and synoptic-scale waves (Luo et al., 2007, 2008, 2018).

At middle to high latitudes, synoptic eddies (SEs) with short (2–8 day periods) time scales can interact with atmospheric LF variability of intermediate (greater than 2 week periods) time scales (Blackmon, Lee, & Wallace, 1984; Blackmon, Lee, Wallace, & Hsu, 1984). It has been recognized that both dynamical and thermal SE feedbacks play crucial roles in modulating extratropical LF variability (e.g., Branstator, 1992, 1995; Cai & Mak, 1990; Jin, 2010; Jin et al., 2006a, 2006b; Lau, 1988; Lau & Holopainen, 1984; Lau & Nath, 1991; Limpasuvan & Hartmann, 1999; Lorenz & Hartmann, 2001; Luo et al., 2007; Nakamura & Wallace, 1993; Nie et al., 2019; Pan et al., 2006; Ren et al., 2009, 2011, 2012; Zhang et al., 2012; Zhou & Ren, 2017; Zhou et al., 2017). Anomalous SE activity could give rise to the growth and maintenance of extratropical LF variability (Deweaver & Nigam, 2000; Hoskins et al., 1983; Kok et al., 1987; Luo, 2005; Song, 2016; Tan et al., 2014, 2015; Vautard et al., 1988; Watanabe, 2009). For example, under constraints of the hydrostatic and quasi-geostrophic balances, both eddy vorticity flux and eddy heat (EH) flux could create a

streamfunction (SF) tendency and potential temperature (PT) tendency through eddy transports as well as secondary circulation. Specifically, the SF tendencies associated with eddy vorticity fluxes are of the same sign throughout the troposphere, while SF tendencies associated with EH fluxes in the upper troposphere are of the opposite sign to those in the lower troposphere (Lau & Holopainen, 1984; Lau & Nath, 1991). EH fluxes can transport positive contributions associated with eddy vorticity fluxes from the upper troposphere to the lower troposphere, thus, maintaining the equivalent barotropic structure of the LF flow (Ren et al., 2011). Temperature tendencies associated with EH fluxes are much stronger than those associated with eddy vorticity fluxes (Lau & Holopainen, 1984), and negatively contribute to local background temperature anomalies (Lau & Nath, 1991; Ren et al., 2011). Efficiency of dynamical SE feedbacks can be quantified through the empirical eddy-induced growth rate developed by Ren et al. (2011) on the basis of the theory of eddy-induced instability of LF variability of Jin (2010). Low-frequency variability can also generate anomalous SE activity, which promotes different kinds of SE feedback (Branstator, 1995; Kug & Jin, 2009; Nakamura & Wallace, 1990; Shutts, 1983). Ren et al. (2009, 2012) proposed a method of eddy structure decomposition to detect how LF flow organizes SE activity to generate SE feedback. This dynamical diagnosis highlights changes in eddy structure, thus facilitating the study of mechanisms behind SE feedback.

Eddy structure decomposition has been used to examine mechanisms behind dynamical SE feedback in the NAO/PNA (Pacific North American pattern) (Ren et al., 2009, 2012; Zhou et al., 2017), while little attention has been given to thermal SE feedback. Lau and Wallace (1979) concluded that EH flux is down gradient of the ambient anomalous time-mean temperature, and that its magnitude does not quite depend on intensity of the local time-mean temperature gradient. Kug et al. (2010) found a so-called left-hand rule whereby EH flux tends to be directed to the left of the LF flow. However, mechanisms through which the

EH flux is generated by LF variability and through which the EH flux modulates the LF thermodynamic structure remain unclear.

It has been widely recognized that the atmosphere's thermodynamic structure plays an essential role in the influence of the NAO on weather and climate over the North Atlantic and even the entire Northern Hemisphere (Hurrell, 1995a; Hurrell et al., 2003; Ogi et al., 2003; Sung et al., 2006; Zuo et al., 2013), and that the NAO is modulated by eddy feedback (Hurrell, 1995b; Luo et al., 2007; Nie et al., 2019; Song, 2016; Tan et al., 2014). Therefore, in this study, we examine the relationship between EH flux and NAO. On the basis of studies that have focused on interactions between eddy vorticity forcing and NAO (Ren et al., 2009, 2012), we explore the mechanisms through which the winter-mean NAO-related thermodynamic structure of the atmosphere is modulated by EH feedback. This paper is organized as follows: data and methodology are introduced in Section 2. Section 3 presents NAO-related PT anomaly and associated EH forcing. The relationship between the LF NAO flow and EH flux is examined in Section 4, and the mechanisms of EH feedback on NAO-related PT anomaly field are examined in Section 5. Asymmetry of EH feedback under positive and negative NAO is discussed in Section 6. Summary and discussions are given in Section 7.

2 Data and methodology

2.1 Reanalysis data and NAO index

In this study, we used daily and monthly mean ERA-Interim reanalysis data (Dee et al., 2011) from January 1979 to December 2017 with a horizontal resolution of $2.5^{\circ} \times 2.5^{\circ}$. These include air temperature, zonal and meridional winds at 12 isobaric levels from 1000 to 100 hPa, and sea level pressure. Zonal and meridional winds were used to derive SF; PT was calculated from air temperature, and was used to avoid the influence of height on the

temperature field. Lanczos band-pass filter (Duchon, 1979) with 41 weights was used to obtain the SE component with 2–8 day periods. All analyses were performed with boreal winter means—mean value from December to the following February (DJF)—from 1979/80 to 2016/17. Seasonal mean anomalies were calculated by subtracting climatology of all the winter data from the original variables; the results are referred to as LF variability.

Values of the NAO index, calculated by applying the rotated principal component analysis (Barnston & Livezey, 1987) to monthly standardized 500-hPa height anomalies, were obtained from the Climate Prediction Center/National Ocean Atmosphere Administration (<https://www.cpc.ncep.noaa.gov/products/precip/CWlink/pna/nao.shtml>). Wintertime index was constructed by averaging the monthly mean index in DJF. We found 12 years with index values exceeding the mean plus 0.60 standard deviation; composites of these years were used to represent the positive NAO phase. We found 9 years with index values below the mean minus 0.60 standard deviation; composites of these years were used to represent the negative NAO phase.

2.2 Statistics related to EH feedback

To quantify SE heat feedback on LF PT anomalies, EH flux (\vec{F}^{heat}) and its forcing ($-\nabla \cdot \vec{F}^{heat}$) were calculated as follows (Ren et al., 2011):

$$\vec{F}^{heat} = \overline{\vec{V}'\theta'}^a = (\overline{u'\theta'}^a, \overline{v'\theta'}^a), \quad (1)$$

$$-\nabla \cdot \vec{F}^{heat} = -\nabla \cdot \overline{\vec{V}'\theta'}^a = \left(\frac{\partial \bar{\theta}^a}{\partial t}\right)_{ed}, \quad (2)$$

where $(\partial \bar{\theta}^a / \partial t)_{ed}$ represents PT tendency induced by anomalous EH fluxes; u' , v' and θ' denote the 2–8-day filtered zonal wind, meridional wind and PT; $\bar{\theta}^a$ represents seasonal mean anomalies; and $\nabla \cdot ()$ is the horizontal divergence operator.

Only the irrotational part of the EH flux— $\vec{F}_{irrot}^{heat} = \nabla \Delta^{-1}(\nabla \cdot \vec{F}^{heat})$ —is taken into consideration because it is the only part that can directly contribute to EH feedback. Here, $\Delta^{-1}()$ is the horizontal Laplacian inversion operator and $\nabla()$ is the horizontal gradient operator.

To quantify the efficiency of EH feedback, the eddy-heat-induced growth (EHG) rate of the LF PT variability was calculated as follows:

$$\lambda = \frac{\iint_S \bar{\theta}^a (\partial \bar{\theta}^a / \partial t)_{ed} dx dy}{\iint_S \bar{\theta}^a \bar{\theta}^a dx dy} \quad (3)$$

This refers to the formula proposed by Ren et al. (2011, 2014) to quantify the efficiency of eddy vorticity feedback. It expresses the ratio between the projection of the eddy-induced LF tendency onto LF variability and the variance of LF variability. The sign indicates whether feedback is positive or negative, and the absolute value indicates the efficiency of the EH feedback. The domain of horizontal integration (S) was specified as the North Atlantic region (100 °W–30 °E, 30 °N–80 °N).

2.3 Partial correlation analysis

Partial correlation was used to examine the independent relationship between synoptic EH flux (denoted as X) and LF variability (denoted as Y) after removal of the influence of a third factor (denoted as Z). The partial correlation coefficient was calculated as follows:

$$r_{XY|Z} = \frac{r_{XY} - r_{XZ}r_{YZ}}{\sqrt{(1-r_{XZ}^2)(1-r_{YZ}^2)}}, \quad (4)$$

where r_{XY} , r_{XZ} , and r_{YZ} denote the bivariate correlations between XY , XZ and YZ , respectively.

2.4 Eddy structure decomposition

We used the eddy structure decomposition method proposed by Ren et al. (2012) to examine mechanisms of EH feedback on NAO-related PT anomaly. The weighted three-point covariance method designed by Ren et al. (2009) was used to extract SE structure. Synoptic-scale PT was projected onto SF to obtain the eddy PT structure coupling with SF structure. The normalized one-point covariance fields for eddy SF structure and PT structure were calculated as follows:

$$\hat{\psi}_j(x_j, y_j; x, y, t_s, \tau) = \frac{\overline{\psi'(x_j, y_j, t)\psi'(x, y, t \pm \tau)^{t_s}}}{\sigma_c[\psi'(x_j, y_j)]}, \quad (5.1)$$

$$\hat{\theta}_j(x_j, y_j; x, y, t_s, \tau) = \frac{\overline{\psi'(x_j, y_j, t)\theta'(x, y, t \pm \tau)^{t_s}}}{\sigma_c[\psi'(x_j, y_j)]}, \quad (5.2)$$

where x and y are the spatial coordinates, t represents time, subscript $j = 0, -1, 1$ denotes the primary base point and its upstream and downstream points, τ is time lag (unit: day) with $\tau = 0$ representing peak of eddy life cycle, over bar denotes DJF mean for year t_s , and σ_c stands for climatological standard deviation. We put the primary base point within the North-Atlantic storm track region near the southern center of action of the NAO where SE activity and eddy feedback efficiency are much stronger and higher, thus, allowing SE structure changes induced by NAO variability to be better examined (Ren et al., 2012). Negative centers in the SF covariance field that are closest to the primary base point were chosen as upstream and downstream points, and the weighted three-point covariance field was calculated as follows:

$$\hat{\psi} = \frac{1}{2} \left[\hat{\psi}_0 - \frac{1}{2} (\hat{\psi}_1 + \hat{\psi}_{-1}) \right], \quad \hat{\theta} = \frac{1}{2} \left[\hat{\theta}_0 - \frac{1}{2} (\hat{\theta}_1 + \hat{\theta}_{-1}) \right]. \quad (6)$$

Where $\hat{\psi}$ is the eddy SF structure (unit is consistent with that used for SF) and $\hat{\theta}$ is the eddy PT structure (unit is same as that used for PT). Both terms can be expressed as the sum

of a basic or climatological part, indicated by suffix c , and a part representing anomalies of the eddy structure relative to the basic eddy structure, indicated by suffix a : $\hat{\psi} = \hat{\psi}_c + \hat{\psi}_a$, $\hat{\theta} = \hat{\theta}_c + \hat{\theta}_a$.

The SE velocity structure can be directly obtained from the eddy SF structure by $\hat{V} = k \times \nabla \hat{\psi}$; it can also be expressed as the sum of a basic or climatological part (suffix c) and a part representing anomalies (suffix a): $\hat{V} = \hat{V}_c + \hat{V}_a$. Thus, EH flux structure can be decomposed as follows:

$$\hat{V}\hat{\theta} = \hat{V}_c\hat{\theta}_c + \hat{V}_c\hat{\theta}_a + \hat{V}_a\hat{\theta}_c + \hat{V}_a\hat{\theta}_a. \quad (7)$$

Where $\hat{V}_c\hat{\theta}_c$ (BB term) is the product of basic eddy velocity (\hat{V}_c) and basic eddy PT ($\hat{\theta}_c$), $\hat{V}_c\hat{\theta}_a$ (BA term) is the product of basic eddy velocity and anomalous eddy PT ($\hat{\theta}_a$), $\hat{V}_a\hat{\theta}_c$ (AB term) is the product of anomalous eddy velocity (\hat{V}_a) and basic eddy PT, and $\hat{V}_a\hat{\theta}_a$ (AA term) is the product of anomalous eddy velocity and anomalous eddy PT.

The BB term is comparable to the climatological eddy flux (Ren et al., 2012), and the anomalous EH flux structure can be expressed as: $(\hat{V}\hat{\theta})_a = \hat{V}_c\hat{\theta}_a + \hat{V}_a\hat{\theta}_c + \hat{V}_a\hat{\theta}_a$. The AA term is a small nonlinear term that can be neglected (Ren et al., 2012; Zhou et al., 2017). Therefore, only the BA term ($\hat{V}_c\hat{\theta}_a$) and AB term ($\hat{V}_a\hat{\theta}_c$) are considered, both of which contribute to the anomalous EH flux.

3 NAO-related patterns of PT field and EH forcing

It is widely recognized that the NAO can strongly influence temperatures over the North Atlantic and surrounding regions (Hurrell, 1995a; Hurrell et al., 2003; Loon & Rogers, 1978; Zuo et al., 2016). On the basis of existing studies (Kutzbach, 1970; Li & Wang, 2003; Rogers & Van Loon, 1982), we defined two indices to reflect features of the dominant temperature anomaly over the North Atlantic. These include the first principal component of

the seasonal-mean 2-m temperature anomalies over the North Atlantic (25 °N–80 °N, 100 °W–40 °E) derived from Empirical Orthogonal Function (EOF) analysis (EOF1_T), and the difference between the standardized 2-m temperature anomalies at 35 °N and 65 °N, zonally-averaged over 80 °W–10 °W (Diff_T) (Figure 1a). Interannual variations of these two indices are quite consistent with those of the NAO index, and correlations with the NAO index are high (correlation coefficients of 0.81 for both indices). Thermal and dynamic patterns associated with these two indices (Figures 1c and 1d) are very similar to those associated with the NAO (Figure 1b). These results indicate that the NAO-related seesaw pattern in temperature is an important thermodynamic signature over the North Atlantic.

Because eddy flux modulates LF variability (e.g., Jin et al., 2006a; Lau & Holopainen, 1984; Lau & Nath, 1991), we used NAO-index regressed PT and EH forcing to examine how the NAO-related thermodynamic structure of the atmosphere is modulated by EH flux. Figure 2 shows that in the middle-lower troposphere, negative (positive) PT anomalies are at high latitudes and positive (negative) anomalies are at mid-latitudes during the positive (negative) NAO phase. Divergence (convergence) of EH fluxes could lead to a cooling (warming) tendency over the center of positive (negative) PT anomalies, resulting in a negative EH feedback that weakens NAO-related PT anomalies. In contrast, in the upper troposphere, negative (positive) PT anomalies are at mid-latitudes during the positive (negative) NAO phase; EH fluxes diverge (converge), inducing a cooling (warming) tendency. At high latitudes, EH fluxes converge (diverge) over the center of positive (negative) PT anomalies during the positive (negative) NAO phase. These results indicate that synoptic EH fluxes result in a positive feedback that can maintain NAO-related PT anomalies.

Effects of synoptic EH fluxes on NAO-related PT anomalies vary with isobar levels. Therefore, in the following sections, we examine the mechanisms through which NAO-related PT anomalies are modulated by EH fluxes.

4 Relationship between LF NAO flow and EH fluxes

Studies indicate that the synoptic EH flux tends to be directed to the left of the background LF flow (Kug et al., 2010; Ren et al., 2011), and to transport heat down the ambient anomalous time-mean temperature gradient, weakening the ambient anomalous time-mean temperature patterns (Lau & Wallace, 1979). Using partial correlation analysis, we examined the independent relationship between LF NAO flow and synoptic EH flux after linearly removing the influence of the ambient PT anomaly gradient. Figure 3 shows that zonal LF flow and meridional EH flux are positively correlated, indicating that westerly (easterly) anomalies are closely related to anomalous northward (southward) EH fluxes. Similarly, meridional LF flow and zonal EH flux are negatively correlated, indicating a close relationship between northerly (southerly) anomalies and anomalous eastward (westward) EH fluxes.

These results suggest that, EH flux still follows the left-hand rule throughout the troposphere in spite of disregarding the down-gradient heat transport effect of synoptic eddies, indicating that synoptic EH fluxes are mostly modulated by ambient LF flow rather than ambient PT anomaly gradient related to NAO. EH forcing is of the same sign throughout the troposphere. However, effects of EH flux on NAO-related thermodynamic structure of the upper troposphere are of the opposite sign to those of the middle-lower troposphere; this might be a direct result of LF PT anomalies in the upper troposphere being of the opposite sign to those in the middle-lower troposphere (Figure 2).

5 Anatomy of EH feedback

We used eddy structure decomposition to examine how LF flow organizes SE activity and generates the observed EH feedback. All analyses were conducted at the 850-hPa level because, in the lower troposphere, the NAO-related thermodynamic structure is more regular, and meridional EH transport in the Atlantic (Lau, 1978) and temperature tendency induced by transient EH forcing (Lau & Holopainen, 1984) are stronger.

Figure 4 shows that EH fluxes diverge from the anticyclonic flow and converge into the cyclonic flow. They are directed to the left of the LF flow, and create negative EH feedback on the NAO-related PT anomaly pattern, which appears to be out of phase with the corresponding SF pattern in the lower troposphere. Centers of EH forcing tend to be located upstream of the NAO flow.

5.1 Changes in SE structure under NAO

Studies indicate that the LF flow could change SE structure (Hartmann & Zuercher, 1998; Qin & Robinson, 1992; Ren et al., 2009, 2012; Yu & Hartmann, 1993). Ren et al. (2009) developed a weighted three-point covariance method to examine SE structure and its changes under NAO. Following this approach, Figures 5 and 6 show the entire life cycles of eddy SF and PT structures as well as their changes during positive and negative phases of the NAO. The basic eddy SF structure, $\hat{\psi}_c$, features a wave-packet-like pattern with alternate anticyclonic and cyclonic eddies from upstream to downstream. A SE originates in the upstream region of the NAO, then elongates meridionally and tilts zonally while propagating eastward, and finally decays downstream. Compared with the SF structure, the basic eddy PT structure, $\hat{\theta}_c$, also has alternating warm and cool patterns and a similar life process for its origination, meridional elongation, zonal tilt and decay. However, it is smaller meridionally, and zonally, it has a phase difference of about one-fourth cycle. Storm tracks in the lower

troposphere are upstream of storm tracks in the upper troposphere (Chang et al., 2002).

Therefore, SE activity and structures in the downstream region of the NAO are weaker and more irregular.

Changes in SE structures under NAO modulation are quite small (Ren et al., 2012). Therefore, to make NAO-modulated SE structure changes more visible, we calculated differences between NAO-related and basic SE structure patterns, multiplied the differences by a factor of two, added them to the basic SE structure patterns, and display them in Figures 5, 6, and 7a, b, e and f. Because of the shearing effect of the NAO flow, SE structures primarily change by (clockwise/counterclockwise) zonal slanting and meridional shifting (Ren et al., 2012). Concurring with theoretical studies (e.g., Luo et al., 2007), our results show that differences between the SE structure during the positive and negative phases of the NAO are slight but distinct (not shown). Following Ren et al. (2012), Figure 7 shows features of eddy structure changes during the entire life cycle of an eddy using a center composite scheme. Figures 7a and b show that, under positive NAO, the SF structure (phase line) tilts clockwise and PT structure shifts northward relative to basic or climatological condition. In contrast, under negative NAO, both SF and PT structures tilt counterclockwise and shift southward (Figures 7e and f). Angles between phase lines under negative NAO and climatological conditions are larger than angles between phase lines under positive NAO and climatological conditions, indicating a larger zonal tilt in the eddy structure under negative NAO.

5.2 Decomposition of eddy structures

Studies indicate that the BA and AB terms of anomalous eddy vorticity fluxes are both involved in generating dynamical eddy feedback (Ren et al., 2012; Zhou et al., 2017), and can be directly estimated from the basic and anomalous eddy structures. Therefore, we used the eddy structure decomposition method to examine the mechanisms through which EH

fluxes are organized by the background NAO flow and give rise to EH forcing on NAO-related LF PT anomaly pattern.

Figure 7c shows basic eddy SF structure, $\hat{\psi}_c$, and anomalous eddy PT structure, $\hat{\theta}_a$, under positive NAO; $\hat{\theta}_a$ is positive (negative) at the upper left (right) and lower right (left) corners of the anticyclonic $\hat{\psi}_c$ while $\hat{\theta}_a$ is negative (positive) at the upper left (right) and lower right (left) corners of the cyclonic $\hat{\psi}_c$. Under positive NAO, $\hat{\theta}_a$ has meridional dipoles that are in quadrature with the anticyclones or cyclones in the $\hat{\psi}_c$, favoring formation of meridional EH fluxes. For example, at the upper left (right) corner of the central anticyclone, positive (negative) $\hat{\theta}_a$ and northward (southward) \hat{V}_c can form a northward $\hat{V}_c \hat{\theta}_a$, and similarly, a southward $\hat{V}_c \hat{\theta}_a$ is formed at the lower part of this anticyclone. Figure 8a shows that the BA term ($\hat{V}_c \hat{\theta}_a$) of the EH flux has a relatively strong meridional component, and it diverges from the southern lobe of the NAO flow, creating negative feedback on the NAO-related LF PT anomalies. Because the zonal tilt of eddy SF structure is relatively small, anomalous eddy SF structure, $\hat{\psi}_a$, almost coincides with basic eddy PT structure, $\hat{\theta}_c$, under positive NAO (Figure 7d), resulting in a weak AB term ($\hat{V}_a \hat{\theta}_c$) (Figure 8b).

Under negative NAO, $\hat{\theta}_a$ also has meridional dipoles that are in quadrature with the anticyclones or cyclones in the $\hat{\psi}_c$ (Figure 7g). As a result, $\hat{V}_c \hat{\theta}_a$ converges into the southern lobe of the NAO flow, creating negative feedback on the NAO-related LF PT anomalies (Figure 8c). Under negative NAO, $\hat{\psi}_a$ shows a meridional in-phase dipole relative to $\hat{\theta}_c$ (Figure 7h); $\hat{\psi}_a$ is positive over the upper (lower) parts of warm (cool) $\hat{\theta}_c$, and $\hat{\psi}_a$ is negative over the lower (upper) parts of warm (cool) $\hat{\theta}_c$, favoring formation of zonal EH fluxes. At the center of the eddy PT structure, positive (negative) $\hat{\theta}_c$ and westward (eastward) \hat{V}_a generate

westward $\hat{V}_a \hat{\theta}_c$ that converge to the west of the southern lobe of NAO flow, inducing an EH forcing upstream of the NAO flow (Figure 8d).

Under both NAO phases, EH forcing induced by AB fluxes is much weaker than that induced by BA fluxes. Therefore, patterns reconstructed from BA fluxes and induced EH forcing (Figure 8) are quite similar to observed patterns (Figure 4), indicating that BA flux is the major contributor to EH forcing. Specifically, under negative NAO, the anomalous eddy SF structure with in-phase dipoles favor formation of zonal AB flux, which further give rise to EH forcing upstream of the NAO flow.

5.3 Mechanisms of EH feedback on NAO

On the basis of our results, we propose a kinematic mechanism of EH feedback on NAO (Figure 9). Without loss of generality, we take the LF cyclonic circulation pattern to represent the southern lobe of the NAO in its negative phase, corresponding to the NAO-related negative PT anomaly pattern in the lower troposphere. There is a phase difference of about one-fourth cycle between the eddy PT and SF structures because of the thermodynamic relationship between meridional wind and temperature on the synoptic scale; this phase difference applies to both basic and anomalous values.

Figure 9a shows that eddy PT structure shifts southward, and is accompanied with eddy SF structure because of the barotropic stretching effect and meridional shifting of local baroclinicity induced by the background NAO flow (Ren et al., 2012). As a result, $\hat{\theta}_a$ has meridional dipoles that are in quadrature with the anticyclones or cyclones in the $\hat{\psi}_c$. In the northern flank of the NAO flow, $\hat{\theta}_a > 0$ ($\hat{\theta}_a < 0$) matching with meridional $\hat{V}_c < 0$ ($\hat{V}_c > 0$) can generate southward $\hat{V}_c \hat{\theta}_a$. Similarly, in the southern flank, $\hat{\theta}_a < 0$ ($\hat{\theta}_a > 0$) matching with meridional $\hat{V}_c < 0$ ($\hat{V}_c > 0$) can generate northward $\hat{V}_c \hat{\theta}_a$. Thus, all the meridional EH

fluxes converge systematically into the NAO cyclonic circulation, weakening the NAO-related negative PT anomaly, thus creating a negative feedback.

The barotropic shearing effect of the background zonal NAO flow can induce zonal slants in the eddy SF structure. Thus, $\hat{\psi}_a$ has meridional dipoles that are in phase with the warm or cool centers in the $\hat{\theta}_c$ (Figure 9b). In the middle latitudes of the NAO circulation, zonal $\hat{v}_a > 0$ ($\hat{v}_a < 0$) matching with $\hat{\theta}_c < 0$ ($\hat{\theta}_c > 0$) can generate westward $\hat{v}_a \hat{\theta}_c$, converging upstream of the NAO flow.

Our results indicate that the BA flux is much larger than the AB flux. Therefore, meridional shifting of the eddy PT structure is primarily responsible for generating EH feedback on NAO.

6 Phase asymmetry of EH feedback on NAO

To further examine EH feedback efficiency, we calculated EHG rate at each isobar level (Figure 10a). Rates of EHG are mainly negative in the middle-lower troposphere but are slightly positive in the upper troposphere, corresponding to the negative and positive EH feedbacks, and is consistent with the results in Section 3. There is a clear asymmetry in EH feedback efficiency; EHG rate in the middle-lower troposphere is negative and has a larger absolute value under positive NAO than under negative NAO; EHG rate in the upper troposphere is positive and is larger under negative NAO than under positive NAO. To understand this phenomenon, we vertically integrated the denominator and numerator of the EHG rate formula (Eqn. 3) over the middle-lower troposphere. Figure 10b shows that, with the exception of one year with a strongly negative NAO, absolute values of numerators in the years of positive NAO are much larger than those in years of negative NAO; values of denominators are similar under the two phases. This indicates that, compared with the negative NAO phase, the projection of EH forcing onto NAO-related PT anomalies under

positive NAO has a much larger absolute value. Under negative NAO, EHG rate is negative with a smaller absolute value, indicating lower EH feedback efficiency and higher persistence of PT anomalies. This may provide new thermodynamic evidence to explain the relative higher persistence of negative NAO (Barnes & Hartmann, 2010; Luo et al., 2018; Woollings et al., 2010) assuming that NAO-related LF flow is intrinsically coupled with the LF PT anomaly. However, differences in the background states (e.g., nonlinearity and energy dispersion) under the two phases of NAO are key factors in NAO asymmetry (Luo et al., 2018), the negatively smaller EHG rate of negative NAO also might be a result of NAO generation. Further in-depth examination are needed in future studies.

7 Summary and discussions

The seesaw pattern of temperature anomalies between the Arctic and subtropical Atlantic is an important indicator of the thermodynamic structure of the NAO. Many studies have shown that SEs could provide feedback on LF variability. This paper focuses on the key role of EH flux and its induced forcing in modulating the NAO-related PT structure, and examines the features and mechanisms of EH feedback.

EH fluxes and their induced forcing are of the same sign throughout the troposphere and are mainly organized by the barotropic NAO flow. However, EH feedback on NAO-related PT anomalies is clearly negative in the middle-lower troposphere and positive in the upper troposphere. This might be a direct result of LF PT anomalies in the upper troposphere being of the opposite sign to those in the middle-lower troposphere.

We used the eddy structure decomposition method to examine the mechanisms of EH feedback on NAO-related PT anomaly. Eddy PT structure is out of phase with eddy SF structure and is shifted meridionally under NAO. The anomalous eddy PT structure has meridional dipoles that are in quadrature with the basic eddy SF structure, forming

meridional BA EH fluxes, which become the major contributor to anomalous EH fluxes and associated EH forcing that are directed to the left of the LF NAO flow. Under negative NAO, the shearing effect of the background zonal NAO flow can induce zonal slants in the eddy SF structure. This creates further changes, and the anomalous eddy SF structure has meridional dipoles that are in phase with the basic eddy PT structure, generating westward zonal AB EH fluxes, which converge and induce further EH forcing upstream of the NAO flow.

Our results show asymmetry in EH feedback under the two NAO phases. Rate of EHG in the middle-lower troposphere is negative and has a larger absolute value under positive NAO than under negative NAO, and is related to the higher persistence of negative NAO. Causes of this asymmetry remain unclear. Future studies should apply the diagnostic framework of the transformed eddy potential vorticity flux (Ren et al., 2011) to take into account the EH-flux-induced dynamic feedback on the two phases of NAO. Besides, considering persistence of NAO on intra-seasonal timescale might be more preferable.

Key climate modes, such as PNA, Arctic Oscillation and Antarctic Oscillation that strongly influence regional and even global weather and climate usually have distinct spatial characteristics and SE feedback processes. The role of EH feedback in modulating LF thermodynamic structures in these climate modes needs to be further explored.

Acknowledgments, Samples, and Data

The daily and monthly mean data used in this work are from ERA-Interim reanalysis data (<https://apps.ecmwf.int/datasets/>). The NAO index is available at the Climate Prediction Center/National Ocean Atmosphere Administration (<https://www.cpc.ncep.noaa.gov/products/precip/CWlink/pna/nao.shtml>). This work was jointly supported by the National Science foundation (NSF) grant of China (Grant Nos. 41775066 and 41375062).

References

- Barnes, E. A., & Hartmann, D. L. (2010). Dynamical Feedbacks and the Persistence of the NAO. *Journal of the atmospheric sciences*, 67(3), 851-865. <https://doi.org/10.1175/2009JAS3193.1>
- Barnston, A. G., & Livezey, R. E. (1987). Classification, Seasonality and Persistence of Low-Frequency Atmospheric Circulation Patterns. *Monthly Weather Review*, 115(6), 1083-1126. [https://doi.org/10.1175/1520-0493\(1987\)115<1083:CSAPOL>2.0.CO;2](https://doi.org/10.1175/1520-0493(1987)115<1083:CSAPOL>2.0.CO;2)
- Blackmon, M. L., Lee, Y. H., & Wallace, J. M. (1984). Horizontal Structure of 500 mb Height Fluctuations with Long, Intermediate and Short Time Scales. *Journal of the atmospheric sciences*, 41(6), 961-980. [https://doi.org/10.1175/1520-0469\(1984\)041<0961:hsomhf>2.0.co;2](https://doi.org/10.1175/1520-0469(1984)041<0961:hsomhf>2.0.co;2)
- Blackmon, M. L., Lee, Y. H., Wallace, J. M., & Hsu, H. H. (1984). Time Variation of 500 mb Height Fluctuations with Long, Intermediate and Short Time Scales as Deduced from Lag-Correlation Statistics. *Journal of the atmospheric sciences*, 41(6), 981-991. [https://doi.org/10.1175/1520-0469\(1984\)041<0981:TVOMHF>2.0.CO;2](https://doi.org/10.1175/1520-0469(1984)041<0981:TVOMHF>2.0.CO;2)
- Branstator, G. (1992). The Maintenance of Low-Frequency Atmospheric Anomalies. *Journal of the atmospheric sciences*, 49(20), 1924-1945. [https://doi.org/10.1175/1520-0469\(1992\)049<1924:TMOLFA>2.0.CO;2](https://doi.org/10.1175/1520-0469(1992)049<1924:TMOLFA>2.0.CO;2)
- Branstator, G. (1995). Organization of Storm Track Anomalies by Recurring Low-Frequency Circulation Anomalies. *Journal of the atmospheric sciences*, 52(2), 207-226. [https://doi.org/10.1175/1520-0469\(1995\)052<0207:OOSTAB>2.0.CO;2](https://doi.org/10.1175/1520-0469(1995)052<0207:OOSTAB>2.0.CO;2)
- Cai, M., & Mak, M. (1990). Symbiotic Relation between Planetary and Synoptic-Scale Waves. *Journal of the atmospheric sciences*, 47(24), 2953-2968. [https://doi.org/10.1175/1520-0469\(1990\)047<2953:SRBPAS>2.0.CO;2](https://doi.org/10.1175/1520-0469(1990)047<2953:SRBPAS>2.0.CO;2)

- Chang, E. K. M., Lee, S., & Swanson, K. L. (2002). Storm Track Dynamics. *Journal of Climate*, 15(16), 2163-2183. [https://doi.org/10.1175/1520-0442\(2002\)015<02163:STD>2.0.CO;2](https://doi.org/10.1175/1520-0442(2002)015<02163:STD>2.0.CO;2)
- Dee, D. P., Uppala, S. M., Simmons, A. J., Berrisford, P., Poli, P., Kobayashi, S., et al. (2011). The ERA-Interim reanalysis: configuration and performance of the data assimilation system. *Quarterly Journal of the Royal Meteorological Society*, 137(656), 553--597. <https://doi.org/10.1002/qj.828>
- Deweaver, E., & Nigam, S. (2000). Zonal-Eddy Dynamics of the North Atlantic Oscillation. *Journal of Climate*, 13(22), 3893-3914. [https://doi.org/10.1175/1520-0442\(2000\)013<3893:ZEDOTN>2.0.CO;2](https://doi.org/10.1175/1520-0442(2000)013<3893:ZEDOTN>2.0.CO;2)
- Duchon, C. E. (1979). Lanczos Filtering in One and Two Dimensions. *Journal of Applied Meteorology*, 18(8), 1016-1022. [https://doi.org/10.1175/1520-0450\(1979\)018<1016:LFIOAT>2.0.CO;2](https://doi.org/10.1175/1520-0450(1979)018<1016:LFIOAT>2.0.CO;2)
- Hartmann, D. L., & Zuercher, P. (1998). Response of Baroclinic Life Cycles to Barotropic Shear. *Journal of the atmospheric sciences*, 55(3), 297-313. [https://doi.org/10.1175/1520-0469\(1998\)055<0297:roblct>2.0.co;2](https://doi.org/10.1175/1520-0469(1998)055<0297:roblct>2.0.co;2)
- Hoskins, B. J., James, I. N., & White, G. H. (1983). The Shape, Propagation and Mean-Flow Interaction of Large-Scale Weather Systems. *Journal of the atmospheric sciences*, 40(7), 1595-1612. [https://doi.org/10.1175/1520-0469\(1983\)040<1595:tspamf>2.0.co;2](https://doi.org/10.1175/1520-0469(1983)040<1595:tspamf>2.0.co;2)
- Hurrell, J. W. (1995a). Decadal Trends in the North Atlantic Oscillation: Regional Temperatures and Precipitation. *Science*, 269(5224), 676-679. <https://doi.org/10.1126/science.269.5224.676>
- Hurrell, J. W. (1995b). Transient Eddy Forcing of the Rotational Flow during Northern Winter. *Journal of the atmospheric sciences*, 52(12), 2286-2301.

[https://doi.org/10.1175/1520-0469\(1995\)052<2286:TEFOTR>2.0.CO;2](https://doi.org/10.1175/1520-0469(1995)052<2286:TEFOTR>2.0.CO;2)

Hurrell, J. W., & Deser, C. (2009). North Atlantic climate variability: The role of the North Atlantic Oscillation. *Journal of Marine Systems*, 79(1), 231-244.

<https://doi.org/10.1016/j.jmarsys.2008.11.026>

Hurrell, J. W., Kushnir, Y., Ottersen, G., & Visbeck, M. (2003). An Overview of the North Atlantic Oscillation. *Geophysical monograph*, 134, 1-35.

<https://doi.org/10.1029/134GM01>

Jin, F. F. (2010). Eddy-Induced Instability for Low-Frequency Variability. *Journal of the atmospheric sciences*, 67(6), 1947-1964. <https://doi.org/10.1175/2009JAS3185.1>

Jin, F. F., Pan, L. L., & Watanabe, M. (2006a). Dynamics of synoptic eddy and low-frequency flow interaction. Part I: A linear closure. *Journal of the atmospheric sciences*, 63(7), 1677-1694. <https://doi.org/10.1175/JAS3715.1>

Jin, F. F., Pan, L. L., & Watanabe, M. (2006b). Dynamics of Synoptic Eddy and Low-Frequency Flow Interaction. Part II: A Theory for Low-Frequency Modes. *Journal of the atmospheric sciences*, 63(7), 1695-1708. <https://doi.org/10.1175/JAS3716.1>

Kok, C. J., Opsteegh, J. D., & Dool, H. M. v. d. (1987). Linear Models: Useful Tools to Analyze GCM Results. *Monthly Weather Review*, 115(9), 1996-2008.

[https://doi.org/10.1175/1520-0493\(1987\)115<1996:lmutta>2.0.co;2](https://doi.org/10.1175/1520-0493(1987)115<1996:lmutta>2.0.co;2)

Kug, J. S., & Jin, F. F. (2009). Left-hand rule for synoptic eddy feedback on low-frequency flow. *Geophysical Research Letters*, 36. <https://doi.org/10.1029/2008gl036435>

Kug, J. S., Jin, F. F., Park, J., Ren, H. L., & Kang, I. S. (2010). A general rule for synoptic-eddy feedback onto low-frequency flow. *Climate Dynamics*, 35(6), 1011-1026.

<https://doi.org/10.1007/s00382-009-0606-8>

- Kutzbach, J. E. (1970). Large-scale features of monthly mean Northern Hemisphere anomaly maps of sea-level pressure. *Monthly Weather Review*, 98(9), 708-716. [https://doi.org/10.1175/1520-0493\(1970\)098<0708:LSFOMM>2.3.CO;2](https://doi.org/10.1175/1520-0493(1970)098<0708:LSFOMM>2.3.CO;2)
- Lau, N. C. (1978). On the Three-Dimensional Structure of the Observed Transient Eddy Statistics of the Northern Hemisphere Wintertime Circulation. *Journal of the atmospheric sciences*, 35(10), 1900-1923. [https://doi.org/10.1175/1520-0469\(1978\)035<1900:OTTDSO>2.0.CO;2](https://doi.org/10.1175/1520-0469(1978)035<1900:OTTDSO>2.0.CO;2)
- Lau, N. C. (1988). Variability of the Observed Midlatitude Storm Tracks in Relation to Low-Frequency Changes in the Circulation Pattern. *Journal of the atmospheric sciences*, 45(19), 2718-2743. [https://doi.org/10.1175/1520-0469\(1988\)0452.0.CO;2](https://doi.org/10.1175/1520-0469(1988)0452.0.CO;2)
- Lau, N. C., & Holopainen, E. O. (1984). Transient eddy forcing of the time-mean flow as identified by geopotential tendencies. *Journal of the atmospheric sciences*, 41(3), 313-328. [https://doi.org/10.1175/1520-0469\(1984\)041<0313:TEFOTT>2.0.CO;2](https://doi.org/10.1175/1520-0469(1984)041<0313:TEFOTT>2.0.CO;2)
- Lau, N. C., & Nath, M. J. (1991). Variability of the Baroclinic and Barotropic Transient Eddy Forcing Associated with Monthly Changes in the Midlatitude Storm Tracks. *Journal of the atmospheric sciences*, 48(24), 2589-2613. [https://doi.org/10.1175/1520-0469\(1991\)048<2589:VOTBAB>2.0.CO;2](https://doi.org/10.1175/1520-0469(1991)048<2589:VOTBAB>2.0.CO;2)
- Lau, N. C., & Wallace, J. M. (1979). On the Distribution of Horizontal Transports by Transient Eddies in the Northern Hemisphere Wintertime Circulation. *Journal of the atmospheric sciences*, 36(10), 1844-1861. [https://doi.org/10.1175/1520-0469\(1979\)036<1844:OTDOHT>2.0.CO;2](https://doi.org/10.1175/1520-0469(1979)036<1844:OTDOHT>2.0.CO;2)
- Li, J. P., & Wang, J. X. L. (2003). A New North Atlantic Oscillation Index and Its Variability. *Advances in Atmospheric Sciences*, 20(5), 661-676. <https://doi.org/10.1007/bf02915394>
- Limpasuvan, V., & Hartmann, D. L. (1999). Eddies and the annular modes of climate

variability. *Geophysical Research Letters*, 26(20), 3133-3136.

<https://doi.org/10.1029/1999gl010478>

Loon, H. V., & Rogers, J. C. (1978). The Seesaw in Winter Temperatures between Greenland and Northern Europe. Part I: General Description. *Monthly Weather Review*, 106(3), 296-310. [https://doi.org/10.1175/1520-0493\(1978\)106<0296:TSIWTB>2.0.CO;2](https://doi.org/10.1175/1520-0493(1978)106<0296:TSIWTB>2.0.CO;2)

Lorenz, D. J., & Hartmann, D. L. (2001). Eddy-Zonal Flow Feedback in the Southern Hemisphere. *Journal of the atmospheric sciences*, 58(21), 3312-3327. <https://doi.org/10.1175/JAS4005.1>

Luo, D. H. (2005). A Barotropic Envelope Rossby Soliton Model for Block–Eddy Interaction. Part I: Effect of Topography. *Journal of the atmospheric sciences*, 62(1), 5-21. <https://doi.org/10.1175/1186.1>

Luo, D. H., Chen, X. D., & Feldstein, S. B. (2018). Linear and Nonlinear Dynamics of North Atlantic Oscillations: A New Thinking of Symmetry Breaking. *Journal of the atmospheric sciences*, 75(6), 1955-1977. <https://doi.org/10.1175/JAS-D-17-0274.1>

Luo, D. H., Gong, T. T., & Zhong, L. H. (2008). Dynamical Relationship between the Phase of North Atlantic Oscillations and the Meridional Excursion of a Preexisting Jet : An Analytical Study. *Journal of the atmospheric sciences*, 65(6), 1838-1858. <https://doi.org/10.1175/2007JAS2560.1>

Luo, D. H., Lupo, A. R., & Wan, H. (2007). Dynamics of Eddy-Driven Low-Frequency Dipole Modes. Part I: A Simple Model of North Atlantic Oscillations. *Journal of the atmospheric sciences*, 64(1), 3-28. <https://doi.org/10.1175/JAS3818.1>

Marshall, J., Kushnir, Y., Battisti, D. S., Chang, P., Czaja, A., Dickson, R., et al. (2001). North Atlantic climate variability: phenomena, impacts and mechanisms. *International Journal of Climatology*, 21(15), 1863-1898. <https://doi.org/10.1002/joc.693>

- Nakamura, H., & Wallace, J. M. (1990). Observed Changes in Baroclinic Wave Activity during the Life Cycles of Low-Frequency Circulation Anomalies. *Journal of the atmospheric sciences*, 47(9), 1100-1116. [https://doi.org/10.1175/1520-0469\(1990\)047<1100:ocibwa>2.0.co;2](https://doi.org/10.1175/1520-0469(1990)047<1100:ocibwa>2.0.co;2)
- Nakamura, H., & Wallace, J. M. (1993). Synoptic Behavior of Baroclinic Eddies during the Blocking Onset. *Monthly Weather Review*, 121(7), 1892-1903. [https://doi.org/10.1175/1520-0493\(1993\)121<1892:SBOBED>2.0.CO;2](https://doi.org/10.1175/1520-0493(1993)121<1892:SBOBED>2.0.CO;2)
- Nie, Y., Ren, H. L., & Zhang, Y. (2019). The Role of Extratropical Air–Sea Interaction in the Autumn Subseasonal Variability of the North Atlantic Oscillation. *Journal of Climate*, 32(22), 7697-7712. <https://doi.org/10.1175/jcli-d-19-0060.1>
- Ogi, M., Tachibana, Y., & Yamazaki, K. (2003). Impact of the wintertime North Atlantic Oscillation (NAO) on the summertime atmospheric circulation. *Geophysical Research Letters*, 30(13), 1704. <https://doi.org/10.1029/2003GL017280>
- Pan, L. L., Jin, F. F., & Watanabe, M. (2006). Dynamics of Synoptic Eddy and Low-Frequency Flow Interaction. Part III: Baroclinic Model Results. *Journal of the atmospheric sciences*, 63(7), 1709-1725. <https://doi.org/10.1175/JAS3717.1>
- Qin, J. C., & Robinson, W. A. (1992). Barotropic dynamics of interactions between synoptic and low-frequency eddies. *Journal of the atmospheric sciences*, 49(1), 71-79. [https://doi.org/10.1175/1520-0469\(1992\)049<0071:BDOIBS>2.0.CO;2](https://doi.org/10.1175/1520-0469(1992)049<0071:BDOIBS>2.0.CO;2)
- Ren, H. L., Jin, F. F., & Gao, L. (2012). Anatomy of Synoptic Eddy–NAO Interaction through Eddy Structure Decomposition. *Journal of the atmospheric sciences*, 69(7), 2171-2191. <https://doi.org/10.1175/JAS-D-11-069.1>
- Ren, H. L., Jin, F. F., & Kug, J. S. (2014). Eddy-Induced Growth Rate of Low-Frequency Variability and Its Mid- to Late Winter Suppression in the Northern Hemisphere.

Journal of the atmospheric sciences, 71(7), 2281-2298. <https://doi.org/10.1175/JAS-D-13-0221.1>

Ren, H. L., Jin, F. F., Kug, J. S., & Gao, L. (2011). Transformed eddy-PV flux and positive synoptic eddy feedback onto low-frequency flow. *Climate Dynamics*, 36, 2357-2370. <https://doi.org/10.1007/s00382-010-0913-0>

Ren, H. L., Jin, F. F., Kug, J. S., Zhao, J. X., & Park, J. (2009). A kinematic mechanism for positive feedback between synoptic eddies and NAO. *Geophysical Research Letters*, 36(11). <https://doi.org/10.1029/2009GL037294>

Rogers, J. C., & Van Loon, H. (1982). Spatial Variability of Sea Level Pressure and 500 mb Height Anomalies over the Southern Hemisphere. *Monthly Weather Review*, 110(10), 1375-1392. [https://doi.org/10.1175/1520-0493\(1982\)110<1375:SVOSLP>2.0.CO;2](https://doi.org/10.1175/1520-0493(1982)110<1375:SVOSLP>2.0.CO;2)

Shutts, G. J. (1983). The propagation of eddies in diffluent jetstreams: Eddy vorticity forcing of 'blocking' flow fields. *Quarterly Journal of the Royal Meteorological Society*, 109(462), 737-761. <https://doi.org/10.1002/qj.49710946204>

Song, J. (2016). Understanding Anomalous Eddy Vorticity Forcing in North Atlantic Oscillation Events. *Journal of the atmospheric sciences*, 73(8), 2985-3007. <https://doi.org/10.1175/jas-d-15-0253.1>

Sung, M. K., Kwon, W. T., Baek, H. J., Boo, K. O., Lim, G. H., & Kug, J. S. (2006). A possible impact of the North Atlantic Oscillation on the east Asian summer monsoon precipitation. *Geophysical Research Letters*, 33(21). <https://doi.org/10.1029/2006GL027253>

Tan, G. R., Jin, F. F., Ren, H. L., & Sun, Z. B. (2014). The role of eddy feedback in the excitation of the NAO. *Meteorological Applications*, 21(3), 768-776. <https://doi.org/10.1002/met.1415>

- Tan, G. R., Ren, H. L., & Chen, H. S. (2015). Quantifying synoptic eddy feedback onto the low-frequency flow associated with anomalous temperature events in January over China. *International Journal of Climatology*, 35(8), 1976-1983. <https://doi.org/10.1002/joc.4135>
- Vautard, R., Legras, B., & Déqué, M. (1988). On the Source of Midlatitude Low-Frequency Variability. Part I: A Statistical Approach to Persistence. *Journal of the atmospheric sciences*, 45(20), 2811-2844. [https://doi.org/10.1175/1520-0469\(1988\)045<2811:otsoml>2.0.co;2](https://doi.org/10.1175/1520-0469(1988)045<2811:otsoml>2.0.co;2)
- Wallace, J. M., & Gutzler, D. S. (1981). Teleconnections in the Geopotential Height Field during the Northern Hemisphere Winter. *Monthly Weather Review*, 109(4), 784-812. [https://doi.org/10.1175/1520-0493\(1981\)109<0784:TITGHF>2.0.CO;2](https://doi.org/10.1175/1520-0493(1981)109<0784:TITGHF>2.0.CO;2)
- Watanabe, M. (2009). Self - limiting feedback between baroclinic waves and a NAO - like sheared zonal flow. *Geophysical Research Letters*, 36(8). <https://doi.org/10.1029/2009GL037176>
- Woollings, T., Hannachi, A., Hoskins, B. J., & Turner, A. G. (2010). A regime view of the North Atlantic Oscillation and its response to anthropogenic forcing. *Journal of Climate*, 23(6), 1291-1307. <https://doi.org/10.1175/2009JCLI3087.1>
- Yu, J. Y., & Hartmann, D. L. (1993). Zonal Flow Vacillation and Eddy Forcing in a Simple GCM of the Atmosphere. *Journal of the atmospheric sciences*, 50(19), 3244-3259. [https://doi.org/10.1175/1520-0469\(1993\)050<3244:ZFVAEF>2.0.CO;2](https://doi.org/10.1175/1520-0469(1993)050<3244:ZFVAEF>2.0.CO;2)
- Zhang, Y., Yang, X. Q., Nie, Y., & Chen, G. (2012). Annular Mode-Like Variation in a Multilayer Quasigeostrophic Model. *Journal of the atmospheric sciences*, 69(10), 2940-2958. <https://doi.org/10.1175/JAS-D-11-0214.1>
- Zhou, F., & Ren, H. L. (2017). Dynamical Feedback between Synoptic Eddy and Low-

Frequency Flow as Simulated by BCC_CSM1.1(m). *Advances in Atmospheric Sciences*,
34(11), 1316-1332. [https://doi.org/10.1175/1520-0442\(2003\)016<4108:SUTAIL>2.0.CO;2](https://doi.org/10.1175/1520-0442(2003)016<4108:SUTAIL>2.0.CO;2)

Zhou, F., Ren, H. L., Xu, X. F., & Zhou, Y. (2017). Understanding positive feedback between PNA and synoptic eddies by eddy structure decomposition method. *Climate Dynamics*, 48, 1-15. <https://doi.org/10.1007/s00382-016-3304-3>

Zuo, J. Q., Li, W. J., Sun, C. H., Xu, L., & Ren, H. L. (2013). Impact of the North Atlantic sea surface temperature tripole on the East Asian summer monsoon. *Advances in Atmospheric Sciences*, 30(4), 1173-1186. <https://doi.org/10.1007/s00376-012-2125-5>

Zuo, J. Q., Ren, H. L., Li, W. J., & Wang, L. (2016). Interdecadal Variations in the Relationship between the Winter North Atlantic Oscillation and Temperature in South-Central China. *Journal of Climate*, 29(20), 7477-7493. <https://doi.org/10.1175/jcli-d-15-0873.1>

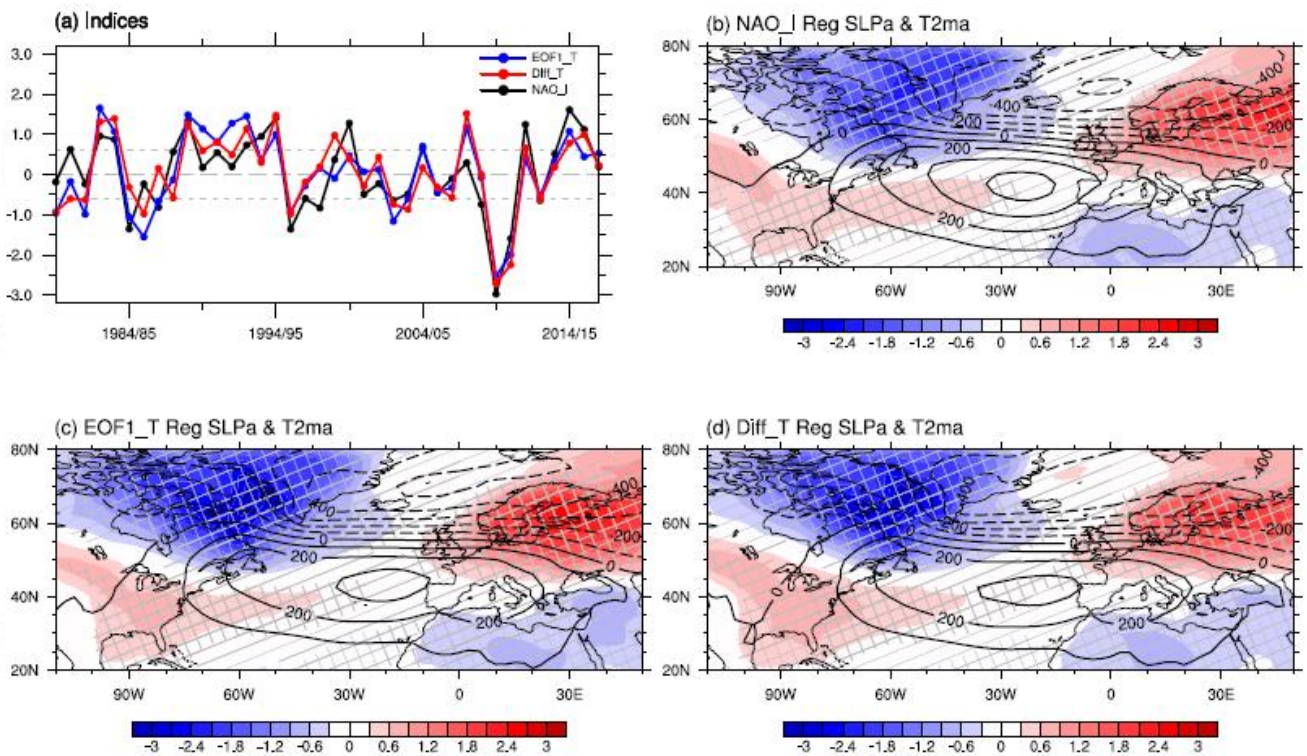


Figure 1. (a) Variation of different indices: standardized NAO index (NAO_I) (black), first principal component of seasonal-mean 2-m temperature anomalies over the North Atlantic (EOF1_T) (blue), and difference between standardized 2-m temperature anomalies at 35 °N and 65 °N, zonally-averaged over 80 °W–10 °W (Diff_T) (red). (b) NAO_I-regressed DJF sea level pressure anomalies (contours, unit: 100 Pa) and 2-m temperature anomalies (shading, unit: 0.3 K). Gray slashes (backslashes) indicate that regressed sea level pressure (2-m temperature) anomalies are significant at the 90% confidence level according to two-tailed Student's *t* tests. (c) same as (b), but for EOF1_T-regressed. (d) same as (b), but for Diff_T-regressed.

Accepted

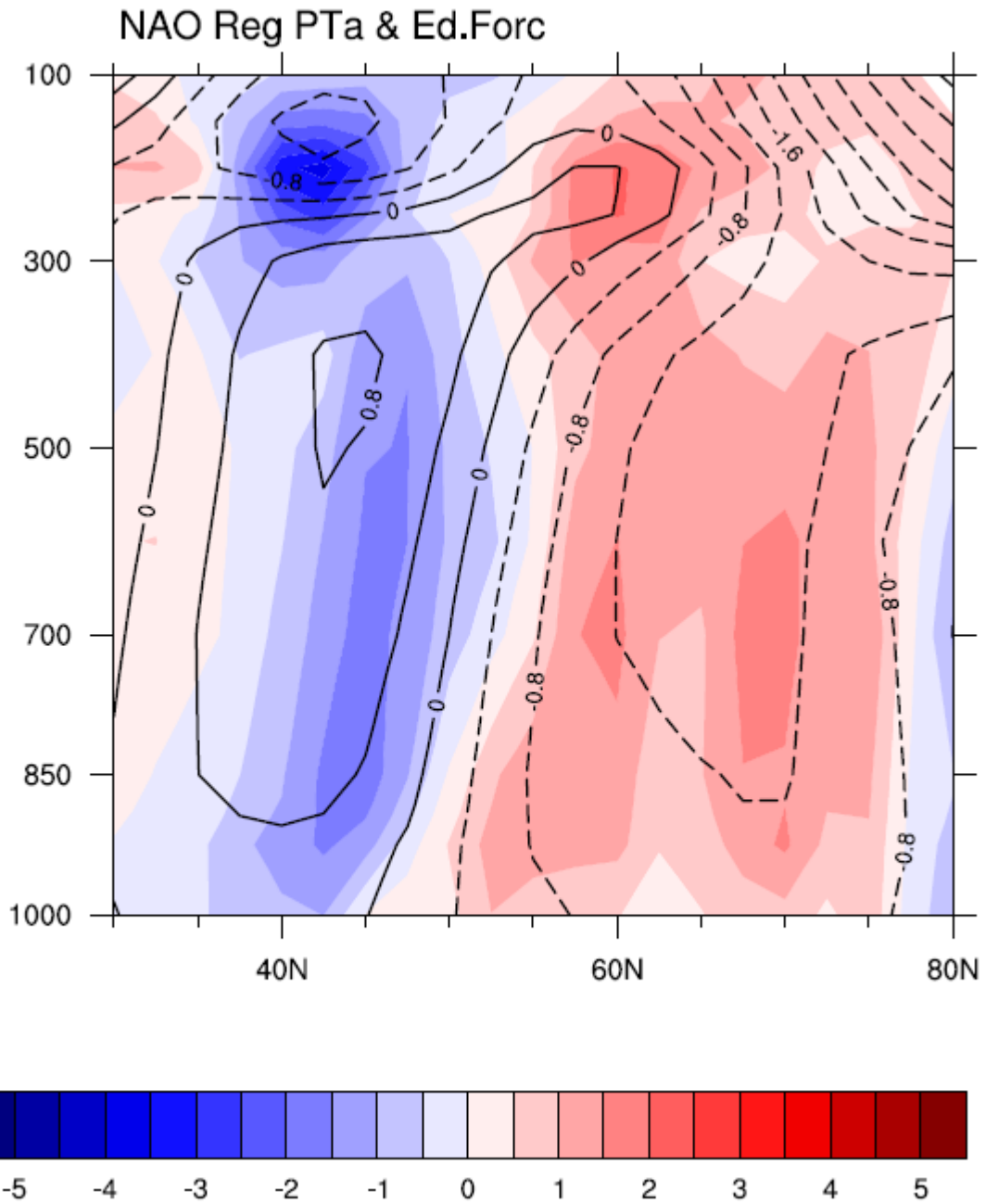


Figure 2. Zonally-averaged vertical–latitude cross sections for NAO-regressed DJF PT anomalies (contours, unit: 0.5 K) and convergences of EH fluxes (shading, unit: $1 \times 10^{-6} \text{ K s}^{-1}$) averaged over the region of $90^\circ \text{W} - 0^\circ$.

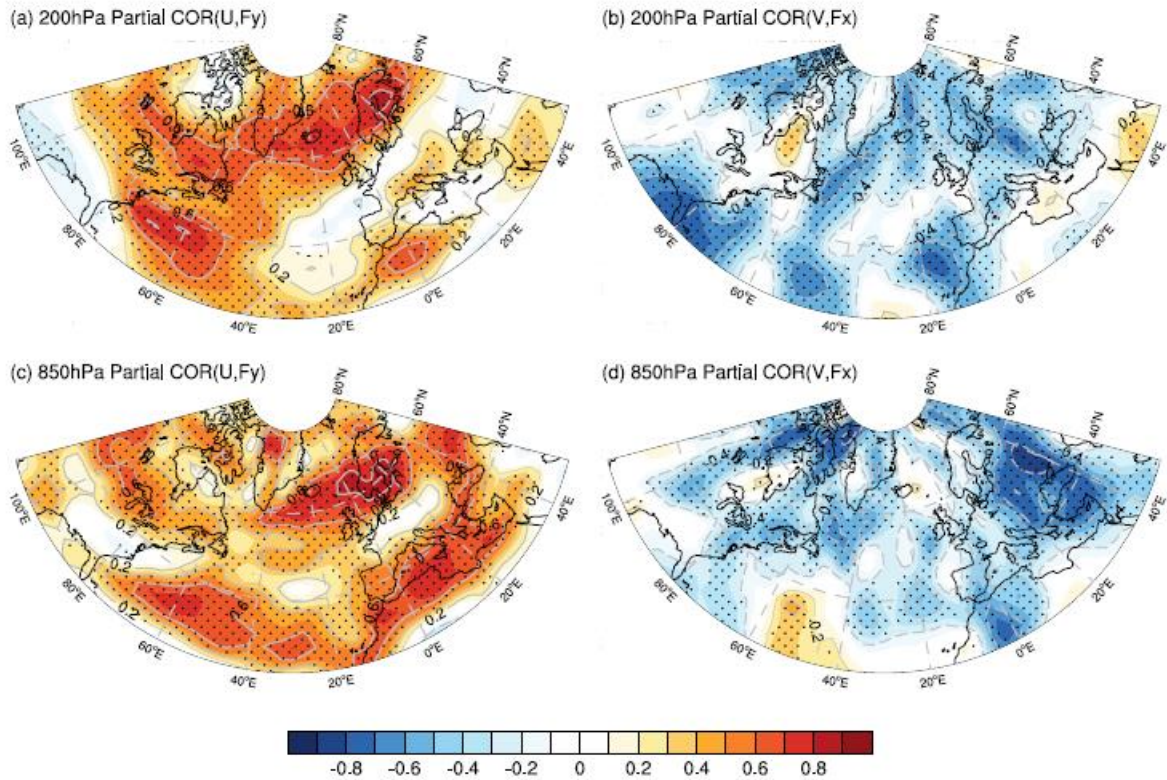


Figure 3. Left panels: partial correlations between DJF zonal LF NAO flow and meridional EH flux after linearly removing the influence of meridional PT anomaly gradient. Right panels: partial correlations between DJF meridional LF NAO flow and zonal EH flux after linearly removing the influence of zonal PT anomaly gradient. At (a–b) 200-hPa level, and (c–d) 850-hPa level. The LF flow, EH flux and PT anomaly gradient have been multiplied by the NAO index to extract the components associated with NAO. Dots indicate that partial correlations are significant at the 90% confidence level according to two-tailed Student's *t* tests.

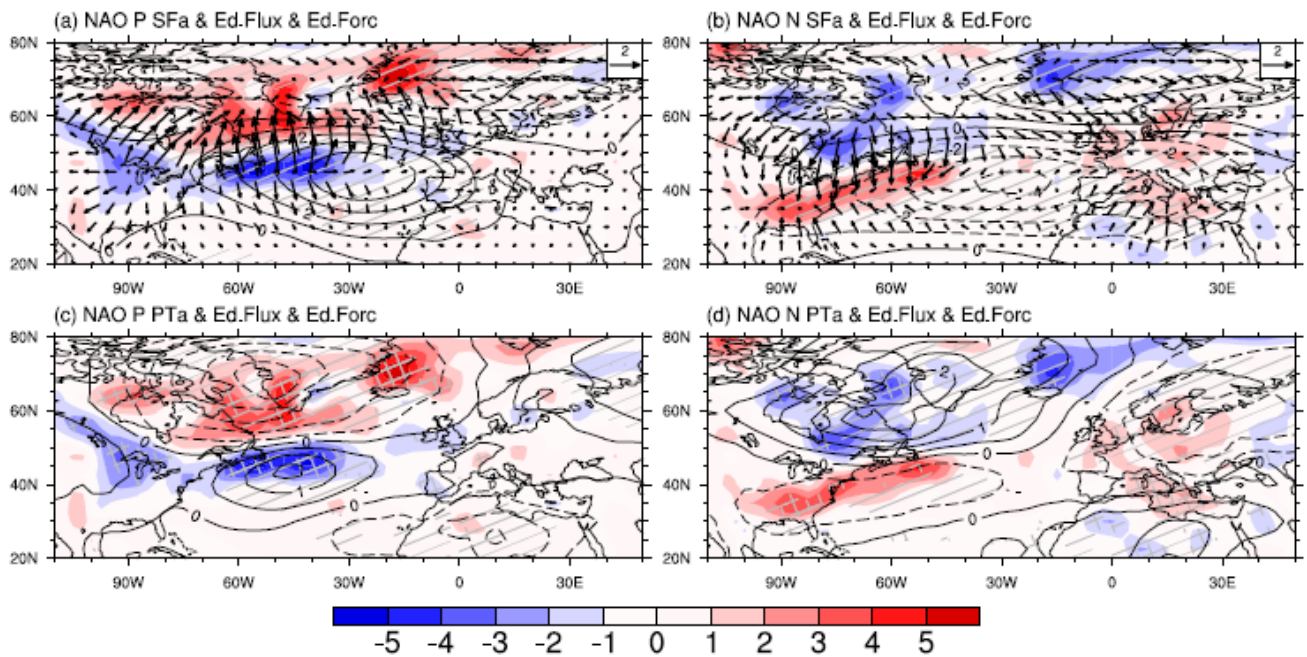


Figure 4. Composite patterns at 850-hPa level. Left panels: positive NAO phase. Right panels: negative NAO phase. Upper panels: anomalous SF (contours, unit: $1 \times 10^6 \text{ m}^2 \text{ s}^{-1}$), convergence of EH fluxes (shading, unit: $1 \times 10^{-6} \text{ K s}^{-1}$), and irrotational component of EH fluxes (vectors, unit: km s^{-1}). Gray slashes indicate that composited anomalous SF is significant at the 90% confidence level according to Student's t tests. Lower panels: anomalous PT (contours, unit: 0.5 K) and convergence of EH fluxes (shading, unit: $1 \times 10^{-6} \text{ K s}^{-1}$). Gray slashes (backslashes) indicate that anomalous composite PT (convergence of EH fluxes) are significant at the 90% confidence level according to two-tailed Student's t tests.

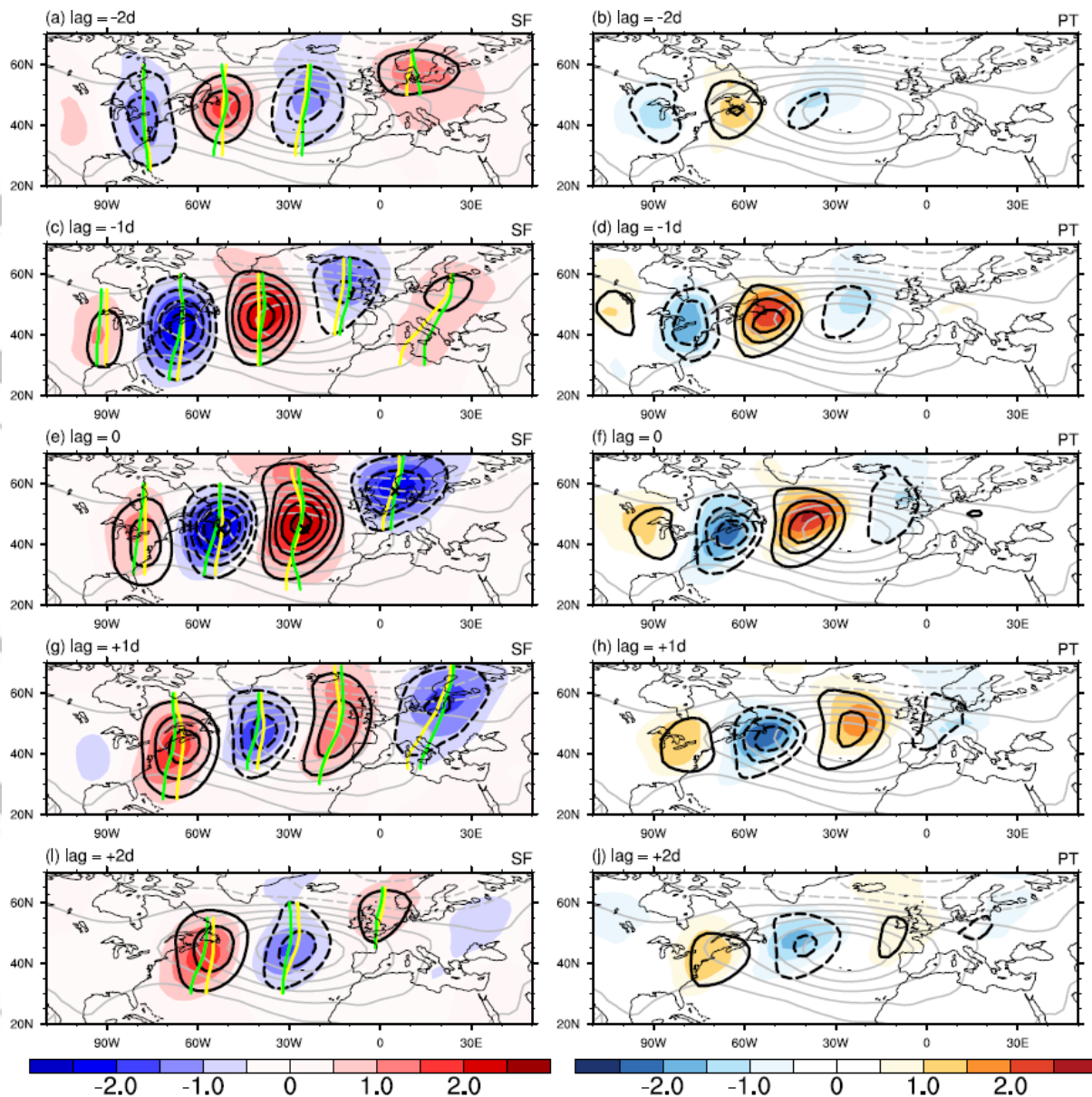


Figure 5. Composite patterns at 850-hPa level. Left panels: Eddy SF structure. Right panels: Eddy PT structure. Black contours indicate basic or climatological condition and shading indicates positive NAO condition. Gray contours denote NAO patterns, as in Figure 4a. Anticyclonic (cyclonic) eddy SF structure patterns are indicated by solid contours and red shading (dashed contours and deep blue shading) at intervals of $0.5 \times 10^6 \text{ m}^2 \text{ s}^{-1}$. Thick curves are phase lines marking zonal extreme of eddy SF structure under basic (yellow) and positive NAO (green) conditions. Positive (negative) eddy PT structure patterns are denoted by solid contours and orange shading (dashed contours and light blue shading) at intervals of 0.5 K. Crosses denote locations of selected base points at 45°N , 335°E ; 45°N , 307.5°E and 57.5°N , 5°E . Top panels show results calculated with lag of -2 days; each panel below shows results calculated with lag of 1 more day; bottom panels show lag of $+2$ days.

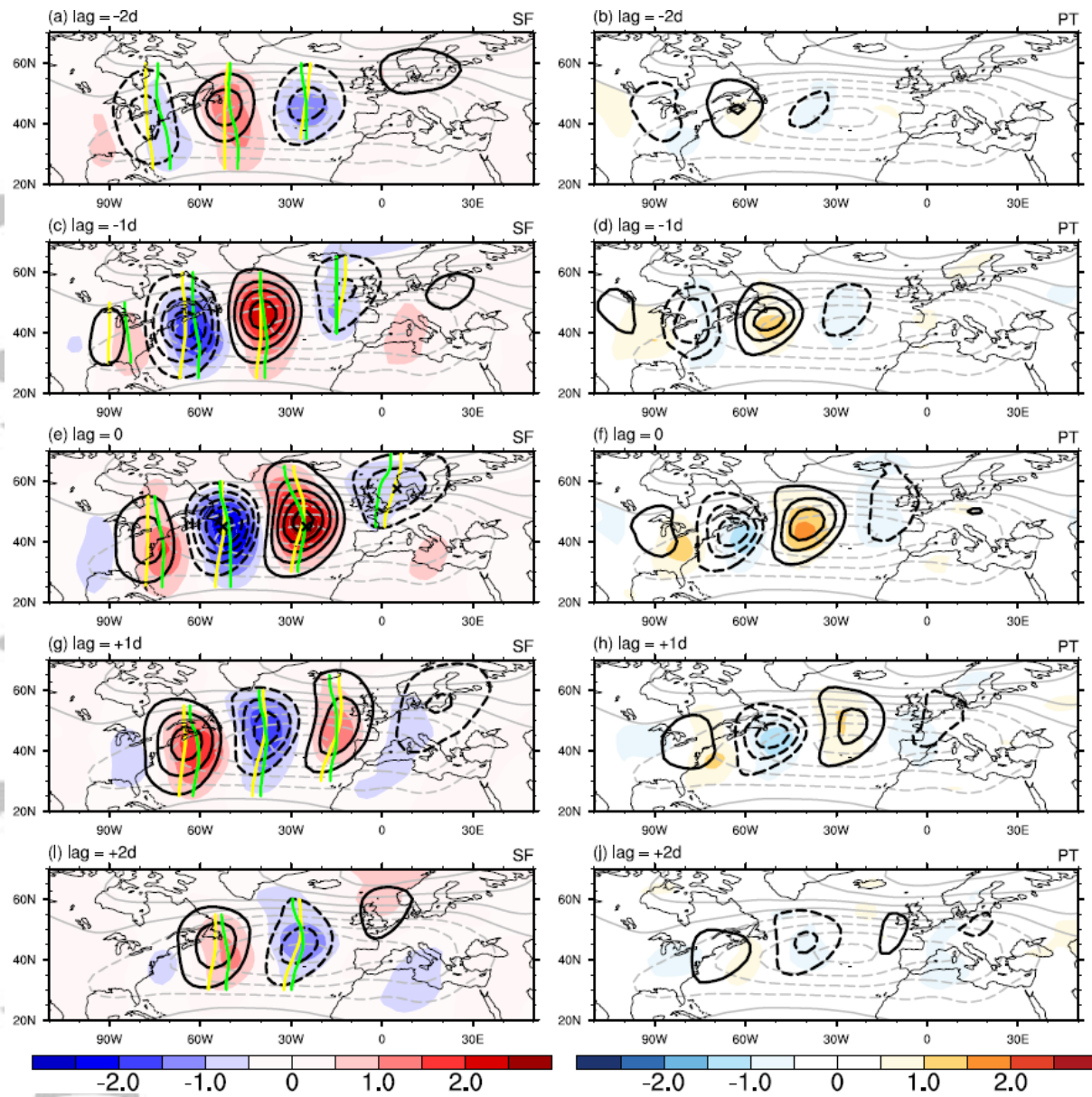


Figure 6. Same as Figure 5, but under negative NAO. Gray contours indicate NAO patterns, as in Figure 4b.

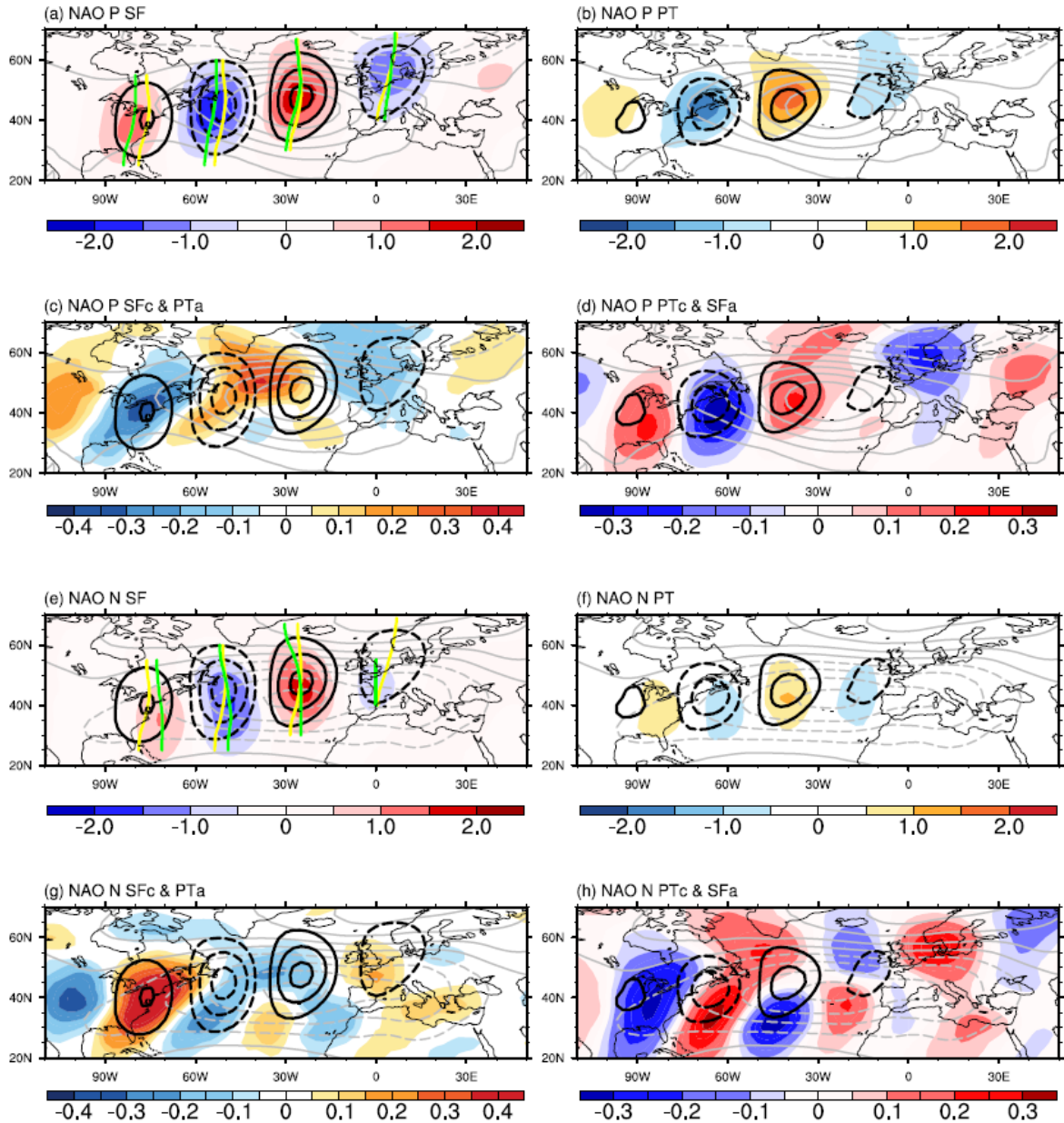


Figure 7. Center composite patterns at 850-hPa level. (a) Eddy SF structure and (b) eddy PT structure generated from the maps with lags of -2 to $+2$ days (Figures 5 a–j) using centers of the central anticyclone and warm eddy at lag of 0 day (Figures 5e and f) under positive NAO and climatological conditions as basic reference points. Black and gray contours, shading and thick curves have the same representations as in Figure 5. (c) Basic eddy SF structure, $\hat{\psi}_c$ (black contours, unit: $0.5 \times 10^6 \text{ m}^2 \text{ s}^{-1}$) and anomalous eddy PT structure, $\hat{\theta}_a$ (shading, unit: 0.05 K) under positive NAO. (d) Basic eddy PT structure, $\hat{\theta}_c$ (black contours, unit: 0.05 K) and anomalous eddy SF structure, $\hat{\psi}_a$ (shading, unit: $0.5 \times 10^6 \text{ m}^2 \text{ s}^{-1}$) under positive NAO. (e–h) same as (a–d), but under negative NAO.

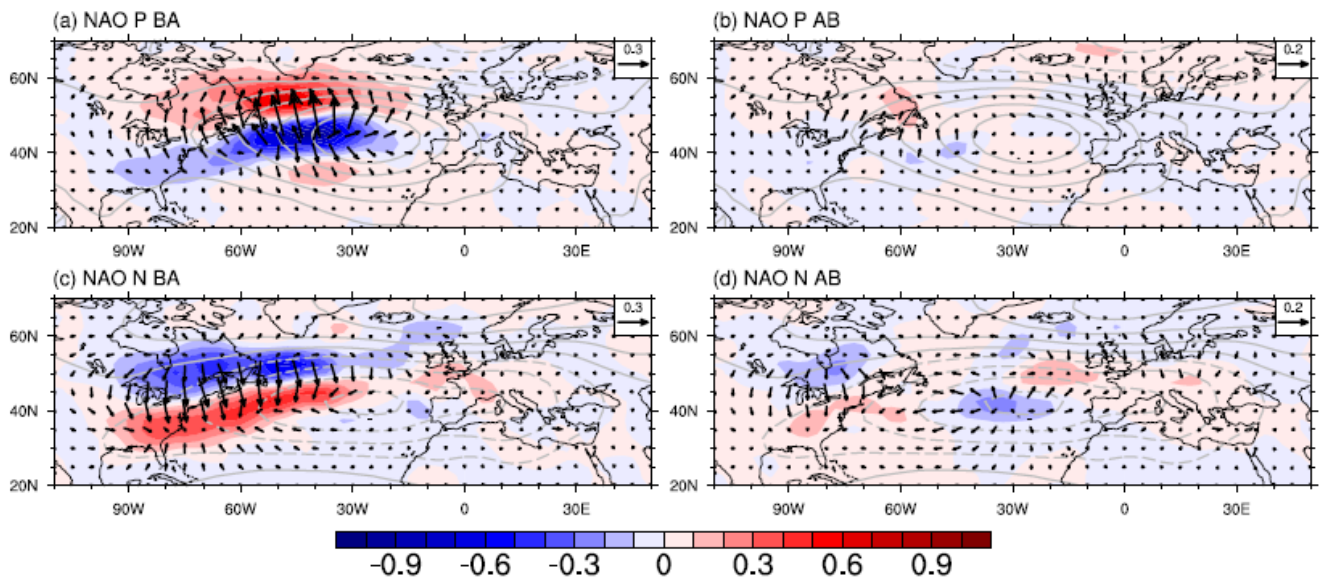


Figure 8. BA and AB terms of the EH flux at 850-hPa level. Left panels: BA term, $\hat{V}_c \hat{\theta}_a$, product of basic eddy velocity and anomalous eddy PT. Right panels: AB term, $\hat{V}_a \hat{\theta}_c$, product of anomalous eddy velocity and basic eddy PT. $\hat{V}_c \hat{\theta}_a$ and $\hat{V}_a \hat{\theta}_c$ are obtained by averaging across the values computed from lags of -2 to $+2$ days (vectors, unit: $K m s^{-1}$). Shading represents associated EH forcing (unit: $1 \times 10^{-6} K s^{-1}$). Gray contours have the same representations as in Figure 5. Upper panels: positive NAO phase. Lower panels: negative NAO phase.

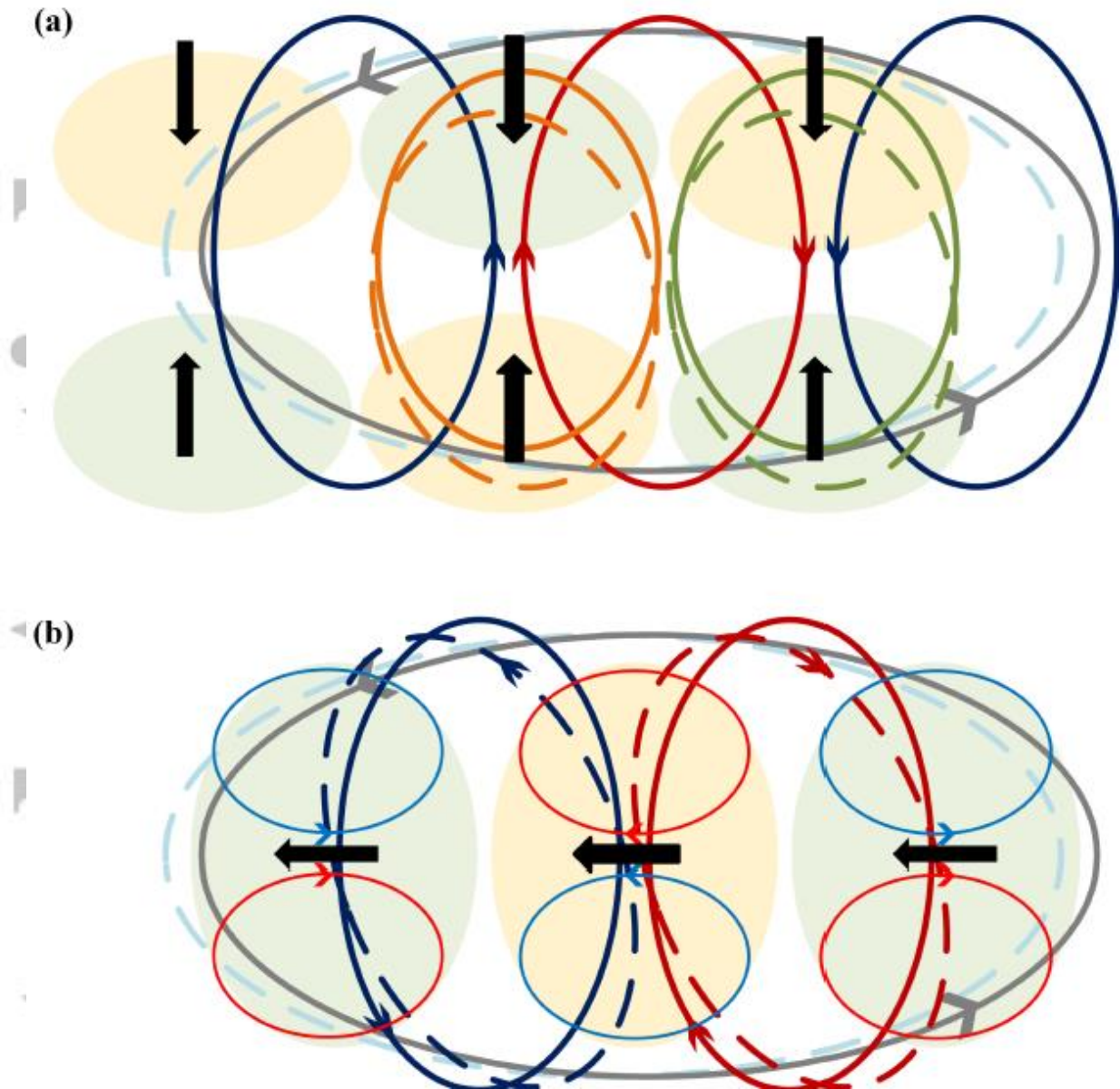


Figure 9. Schematic diagrams of mechanisms of synoptic EH feedback on NAO. Thick gray solid ellipses with counterclockwise arrows represent cyclonic LF flow over the southern lobe of the negative NAO phase. Thin light blue dashed ellipses stand for the corresponding negative PT anomalies in the lower troposphere. Black solid arrows denote the EH fluxes that are larger in the center than two flanks of NAO. (a) Solid thin lines indicate eddy SF structure with cyclonic (deep blue) and anticyclonic (deep red) circulations and eddy PT structure with warm (orange) and cool (deep green) centers. Dashed lines stand for changed eddy PT structure. Shaded ovals denote anomalous PT structures, $\hat{\theta}_a$, with warm (yellow) and cool (green) centers. (b) Solid thin lines indicate eddy SF structure with cyclonic (deep blue) and anticyclonic (deep red) circulations and anomalous SF structures, $\hat{\psi}_a$, with cyclonic (blue) and anticyclonic (red) circulations. Dashed lines stand for changed eddy SF structure. Shaded ovals denote eddy PT structure with warm (yellow) and cool (green) centers.

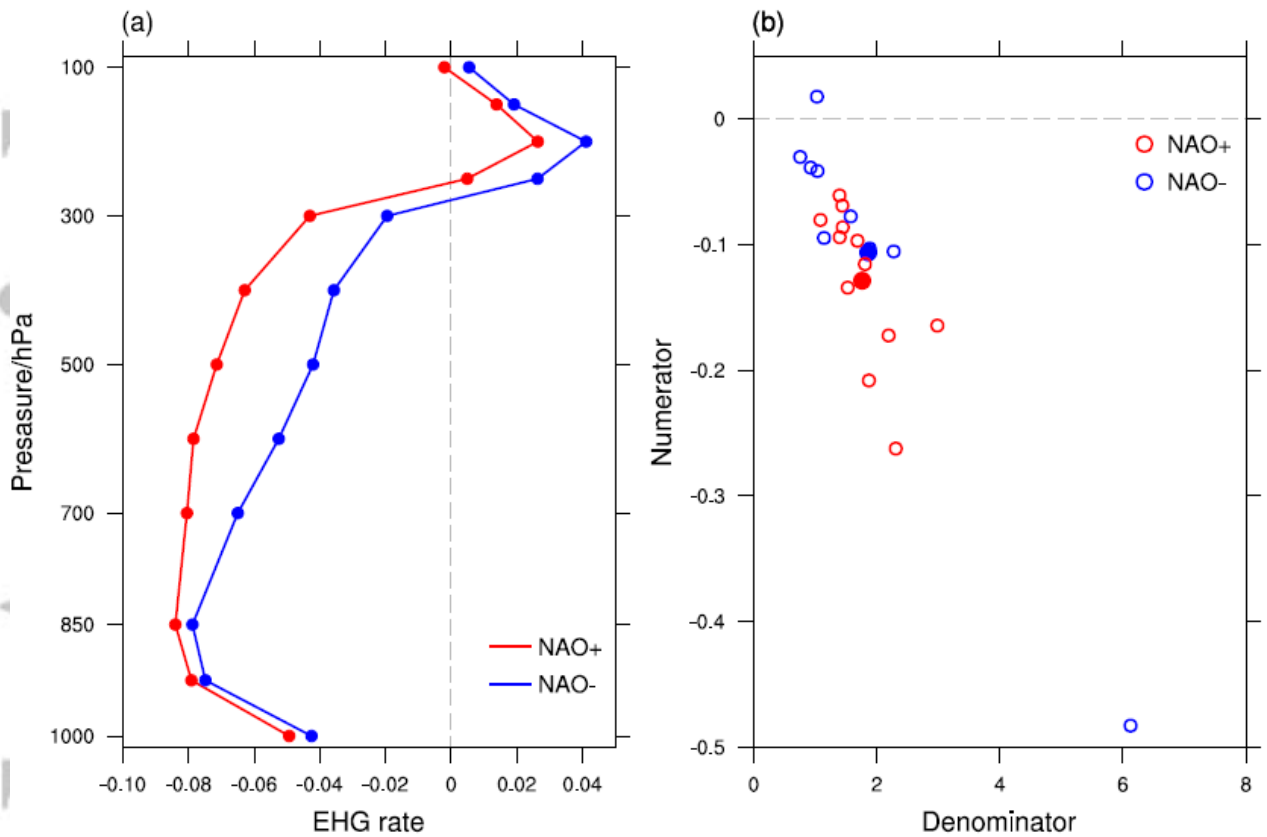


Figure 10. (a) Vertical profiles of EHG rate (unit: d^{-1}) for EH feedback under positive (red) and negative (blue) NAO over the NAO domain. (b) Denominators (x-axes) and numerators (y-axes) of the EHG rate formula (Eqn. 3) vertically integrated over the isobar levels of 850 to 300 hPa for the years with positive (red) and negative (blue) NAO (hollow circles). Shaded circles indicate mean values.